minerals

MDPI

Article

Empirical Study on Reduction Behavior and Metallurgical Properties of Vanadia–Titania Magnetite in Blast Furnace

Zhanwei He [1], Xiaojun Hu [1,*], Mo Lan [1], Jianxing Liu [2], Gongjin Cheng [2], Xiangxin Xue [2,*] and Kouchih Chou [1]

[1] The State Key Laboratory of Advanced Metallurgy, University of Science and Technology Beijing, Beijing 100083, China; b2113767@ustb.edu.cn (Z.H.); G20199312@xs.ustb.edu.cn (M.L.); kcc126@126.com (K.C.)

[2] School of Metallurgy, Northeastern University, Shenyang 110819, China; liujianxing@smm.neu.edu.cn (J.L.); chenggj@smm.neu.edu.cn (G.C.)

* Correspondence: huxiaojun@ustb.edu.cn (X.H.); xuexx@mail.neu.edu.cn (X.X.)

Abstract: The loss of permeability affects the reduction of the ferrous burden in the cohesive zone of a blast furnace (BF). Vanadia–titania magnetite (VTM) burden of various chemical compositions have different metallurgical properties. The reduction and softening-melting-dripping properties of different kinds of VTM were investigated. The results showed that the core of sinter or pellet is indirectly reduced to wustite and (Fe,Ti)O_x, and the periphery contains interlinked metallic iron and $CaSiO_3$ in the cohesive zone. Wustite and (Fe,Ti)O_x are directly reduced in the melting-dripping zone. The aggregate (Fe, V, Cr) present in the non-dripping causes a loss of valuable components. With the increase in TiO_2 content, the substrate phase of molten slag changes from melilite to titanaugite, and the mass of dripping decreases gradually. In addition, the permeability index S increased and the melting zone widened, which indicates that the increase in TiO_2 content negatively affected the melting-dripping performance. The mass of the dripping is directly proportional to the pellet ratio. Considering the adverse effect of TiO_2 on softening-melting-dripping properties, it is recommended that high TiO_2 VTM is smelted while mixed with ordinary ores or with an increased pellet ratio in the burden structure.

Keywords: vanadia–titania magnetite; reduction; softening-melting-dripping property

check for updates

Citation: He, Z.; Hu, X.; Lan, M.; Liu, J.; Cheng, G.; Xue, X.; Chou, K. Empirical Study on Reduction Behavior and Metallurgical Properties of Vanadia–Titania Magnetite in Blast Furnace. *Minerals* **2021**, *11*, 418. https://doi.org/10.3390/min11040418

Academic Editor: Saija Luukkanen

Received: 26 March 2021
Accepted: 13 April 2021
Published: 15 April 2021

Publisher's Note: MDPI stays neutral with regard to jurisdictional claims in published maps and institutional affiliations.

Copyright: © 2021 by the authors. Licensee MDPI, Basel, Switzerland. This article is an open access article distributed under the terms and conditions of the Creative Commons Attribution (CC BY) license (https://creativecommons.org/licenses/by/4.0/).

1. Introduction

Vanadia–titania magnetite (VTM) contains various kinds of valuable elements (Fe, V, Ti, and Cr) and has a high comprehensive utilization value [1,2]. In recent years, the price of vanadium products has remained high, and the smelting of VTM brings huge profits for steel companies. A blast furnace (BF) is the most common method for smelting VTM worldwide [3]. The shape and position of the cohesive zone of the BF, as well as its efficiency, are determined by the melt-down of ores [3,4]. In general, when the thickness of the cohesive zone decreases, the efficiency of the blast furnace increases. The softening and melting temperatures of the burden determine the thickness of the cohesive zone, so the smallest possible difference between them is desired. A reduction degree of a ferrous burden is typically above 50% in the cohesive zone of the BF [4], but the reduction degree of VTM burden is typically lower than this [5]. This leads to the aggravation of the reduction task in the melting-dripping zone. The smelting of VTM is difficult because of the role of titanium in the blast furnace. Thus, the reduction behavior and metallurgical properties of various VTM burden differ from each other markedly.

Titanium is one of the most important influencing factors in the smelting process, which has been studied by domestic and foreign researchers [6–12]. It not only affects the quality and yield of sinter, but also affects the smelting process in the BF. Cheng [13] studied the effect of TiO_2 on the crushing strength and smelting mechanism of high-chromium VTM pellets. It was found that the crushing strength is closely related to the mineral phase

and microstructure, and that the crushing strength decreases when increasing the TiO_2 content. Tang and Zhou [5,14] studied the effect of TiO_2 on the sintering behavior of VTM, which confirmed that the optimum quicklime dosage, mixture moisture, wetting time, and granulation time are 5 wt%, 7.5 wt%, 10 min, and 5–8 min, respectively. Yue [15–17] studied the rheological evolution of Ti-bearing slag with different volume fractions of TiN. It was found that increasing the TiN volume increased the viscosity and the shear stress substantially. Ledzki [18] investigated the potential for the formation of high melting titanium compounds in the metal-slag system by TiO_2 reduction from slag phase by solid carbon and carbon dissolved in iron. Furthermore, the abovementioned studies have focused on the agglomeration or metallurgical properties of the specific VTM under laboratory conditions.

In this work, the reduction behavior of VTM was explained by analyzing the phase composition and microstructure of slag, non-dripping, and dripping at various stages. The empirical studies on the reduction behavior and metallurgical properties of varieties of VTM provide a theoretical basis and technical support for BF smelting VTM.

2. Experimental

2.1. Raw Materials

V–Ti sinter and V–Ti pellet were used in this research as ferrous materials, which were obtained from multiple iron and steel companies in China. The chemical compositions of the ferrous materials and mixed burden (pellet ratio: HJ-45%, CJ-29%, PJ-12.6%) are listed in Table 1. The V-bearing phase is Fe_2VO_4, and the Ti-bearing phase is Fe_2TiO_4, $FeTiO_3$, and Fe_2TiO_5 in sinter and pellet. The chemical compositions of coke are listed in Table 2. The sizes of the V–Ti sinter, V–Ti pellet, and coke were all 10–12.5 mm. All samples were dried at 110 °C.

Table 1. Chemical compositions of ferrous materials and mixed burden.

Items	TFe/wt%	V_2O_5/wt%	TiO_2/wt%	Cr_2O_3/wt%	CaO/wt%	SiO_2/wt%	Al_2O_3/wt%	MgO/wt%	CaO/SiO_2
HJ Sinter	46.98	0.36	1.63	0.25	16.28	5.40	1.91	3.04	3.01
CJ Sinter	56.58	0.37	1.92	0.22	11.03	5.62	1.53	3.70	1.96
PJ Sinter	50.20	0.37	7.88	0.11	9.99	5.71	3.17	2.57	1.75
HJ Pellet	60.83	0.64	2.68	0.64	0.58	6.37	2.48	2.06	0.09
CJ Pellet	59.71	0.52	4.91	0.32	1.93	5.01	1.71	1.57	0.39
PJ Pellet	53.41	0.52	9.90	0.22	1.91	6.11	3.55	2.50	0.31
HJ Burden	53.21	0.49	2.10	0.43	9.22	5.84	2.17	2.60	1.58
CJ Burden	57.49	0.41	2.79	0.25	8.39	5.44	1.58	3.08	1.54
PJ Burden	50.60	0.39	8.13	0.12	8.97	5.76	3.22	2.56	1.56

Table 2. Chemical composition of coke.

Fixed Carbon /wt%	Volatile/wt%	SiO_2/wt%	CaO/wt%	MgO/wt%	Al_2O_3/wt%	S/wt%	Others/wt%
84.58	0.50	7.50	0.48	0.15	2.72	0.492	3.578

2.2. Experiment Methods

Softening-melting-dripping experiments were carried out on the samples to measure their high-temperature properties. The schematic experimental apparatus is shown in Figure 1a. The device comprises a heating system, a gas control system, a temperature control system, and a data recording system. $MoSi_2$ heating elements were used as the core components in the heating system to heat and melt the burden. An R-type thermocouple was placed at the bottom of the compression bar to control the experimental temperature.

The crucible and compression bar were both made of graphite. The dimensions of the crucible are shown in Figure 1b.

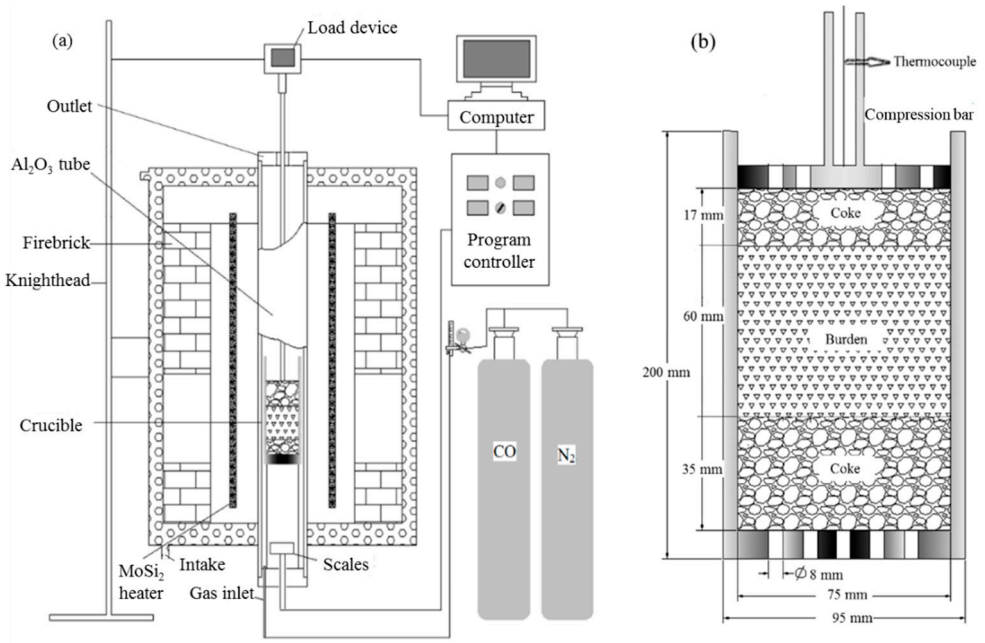

Figure 1. Schematic of the experimental apparatus. (**a**) Apparatus constitute (**b**) Crucible dimensions and charging method.

In order to simulate the blast furnace burden conditions, 500 g of mixed burden was put in the crucible and layers of coke with a depth of 35 mm and 17 mm were placed below and above the samples, respectively. The displacement sensor measured the displacement changes and contraction of the burden when the experiment started. Experimental conditions are shown in Table 3. The heating rates were 10 °C/min below 900 °C, 2 °C/min from 900 °C to 1100 °C, and 5 °C from 1100 °C to the end. To better understand the reduction behavior and softening-melting characteristics of the mixed burden, an interrupted test was also carried out at 1300 °C. The gas was stopped, and N_2 was introduced immediately to prevent the reaction from continuing after the test. When the temperature drops to room temperature, the soft slag, molten slag, non-dripping, and dripping products were collected. The chemical composition and microstructure of collected samples were analyzed by chemical analysis and scanning electron microscopy/energy dispersive X-ray spectroscopy (SEM-EDS).

Table 3. Temperature profile and reduction atmosphere of experiment.

Temperature (°C)	0–500	500–900	900–1100	1100–End
Heating rate (°C/min)	10	10	2	5
Heating time (min)	50	40	100	100
Gas composition and flow rate ($L \cdot min^{-1}$)	100% N_2, 5	70% N_2, 3.5; 30% CO, 1.5		

3. Results and Discussion

3.1. Reduction Behavior of Cohesive Zone

The experiment is terminated when the Burden is heated to 1300 °C, at which point the soft slag in the crucible is taken out. Figure 2a shows the macroscopic morphology of the soft slag. Under the action of external pressure, the upper coke moves downward, and a small amount of molten slag with good fluidity fills the upper coke void, so that the soft slag has been melted into a whole. The outermost edge of the soft slag is a ring of metal shell. When the soft slag is broken, it can be seen from a cross section that the interior is

compact, and that the original shape of sinter and pellet are faintly visible with a metal layer between them. Therefore, the outer edge of sinter and pellet is the first to be reduced.

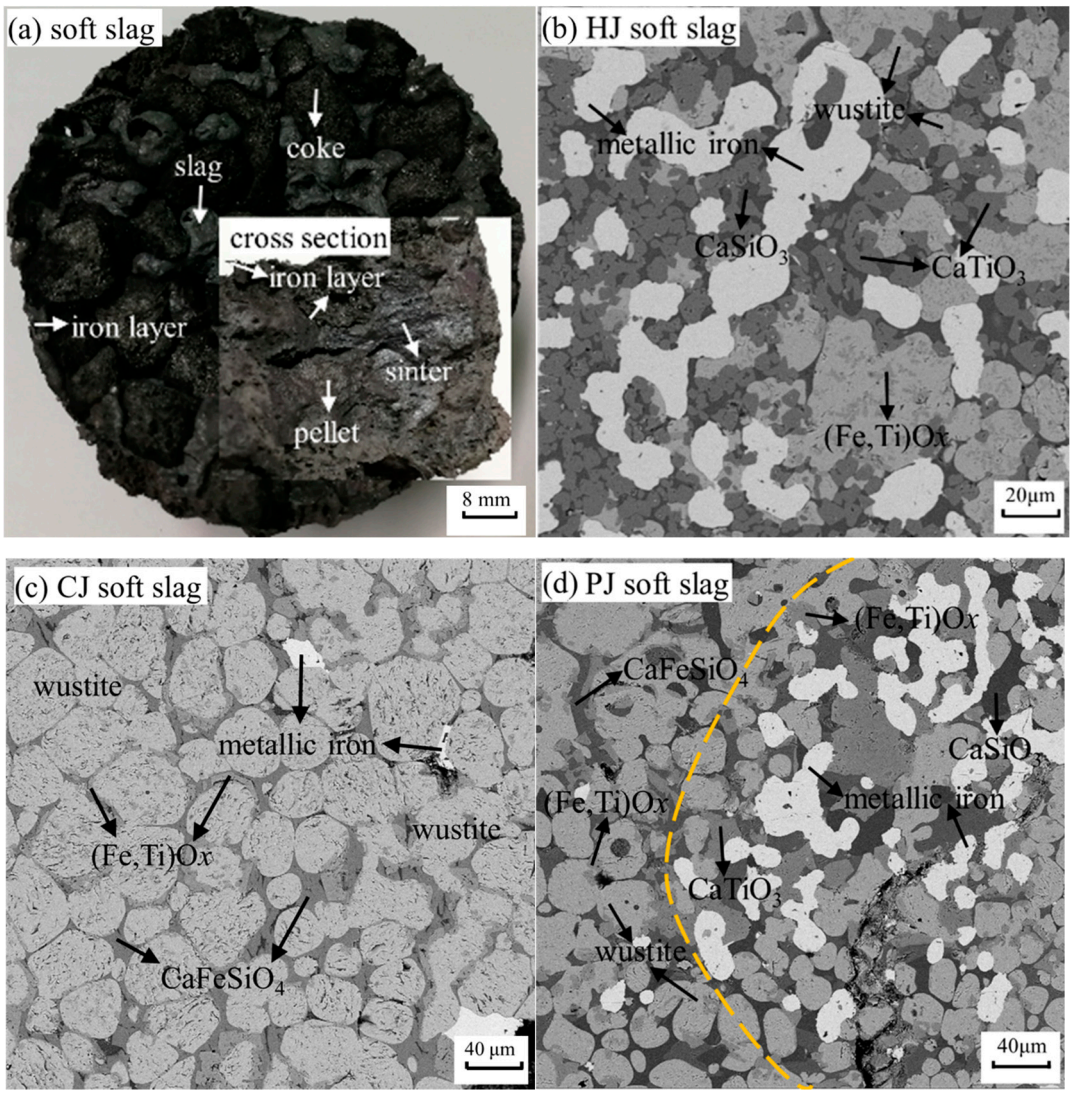

Figure 2. The macroscopic morphology and scanning electron microscope (SEM) images of soft slag: (**a**) Macroscopic morphology; (**b**) SEM image of HJ soft slag; (**c**) CJ soft slag; (**d**) PJ soft slag.

Figure 2b–d shows the SEM images of HJ, CJ, and PJ soft slag. The HJ soft slag is compact and consists mostly of wustite, $CaTiO_3$, metallic iron, and $CaSiO_3$. Some small phases of (Fe,Ti)O_x are found in the wustite. The metallic iron particles diffuse in the slag and are connected to each other, forming a relatively long strip structure. The CJ soft slag is mainly composed of wustite, metallic iron, $CaFeSiO_4$, and (Fe,Ti)O_x. The wustite particles are connected to each other, forming a relatively uniform structure. The (Fe,Ti)O_x phase surrounds the wustite. The small phase of metallic iron is embedded in the slag. In the SEM image of PJ slag, the area to the left of the dotted line consists mostly of wustite, (Fe,Ti)O_x, and $CaFeSiO_4$, while the area to the right includes wustite, $CaTiO_3$, $CaSiO_3$, and (Fe,Ti)O_x.

By comparing the SEM images, there are only a few grains of metallic iron in the CJ soft slag and the left part of the PJ soft slag, suggesting that this portion of the sample is inside the sinter or pellet, which does not make contact with the coke so that it is only being indirectly reduced. The indirect reduction reaction equations are shown in Equations (1)–(3). In the HJ soft slag and the right part of the PJ soft slag, the long strips of metallic iron divide (Fe,Ti)O_x into irregular shapes. The silicates surrounding the metallic iron are mainly $CaSiO_3$. The chemical reaction equations are shown in Equations (4)–(5). It

can be found that iron oxide is indirectly reduced by CO to form (Fe,Ti)O_x and Fe. (Fe,Ti)O_x and $CaFeSiO_4$ are directly reduced by C to form Fe and $CaSiO_3$, respectively.

$$3Fe_2O_3 + CO = 2Fe_3O_4 + CO_2 \quad (1)$$

$$Fe_3O_4 + CO = 3FeO + CO_2 \quad (2)$$

$$FeO + CO = Fe + CO_2 \quad (3)$$

$$FeO + C = Fe + CO \quad (4)$$

$$CaO{\cdot}FeO{\cdot}SiO_2 + C = CaO{\cdot}SiO_2 + Fe + CO \quad (5)$$

3.2. Reduction Behavior of Melting-Dripping Zone

When the Burden reaches the drop temperature, it begins to drop. After 30 min, the experiment ends and the samples in the graphite crucible and bowl are taken out. Figure 3 shows the macroscopic morphology for the molten slag, non-dripping, and dripping. Under the action of external pressure, the molten slag overflows from the small holes and sits on top of the tableting after cooling. The surface of the molten slag is relatively smooth and dense, as shown in Figure 3a. The mobility of the non-dripping is so poor that it cannot drip and stay at the bottom of the crucible. Figure 3b shows that the non-dripping is a dense metal block with coke embedded in it. The dripping drips from the crucible into the graphite bowl. Due to the action of gravity, the dripping is scattered by sputtering, and the surface is in the form of small particles, as shown in Figure 3c.

Figure 3. The macroscopic morphology of samples: (**a**) molten slag; (**b**) non-dripping; (**c**) dripping.

The SEM-EDS images of the HJ, CJ, and PJ molten slag are shown in Figure 4. The HJ molten slag has a simple structure and its base phase is melilite, which mainly consists of Mg, Al, Si, Ca and O. The small metallic iron and $CaTiO_3$ is embedded in the melilite. In Figure 4b, the CJ molten slag mainly consist of melilite, titanaugite, and $CaTiO_3$. The $CaTiO_3$ is embedded in the melilite in the form of granules and leaves. In the PJ molten slag, it can be seen that $CaTiO_3$ particles are connected to each other and that their particle sizes are large. The basal phase titanaugite consist of O, Mg, Al, Si, Ca, and Ti. The metallic iron is embedded in the titanaugite. The TiC phase surrounds the metallic iron particles.

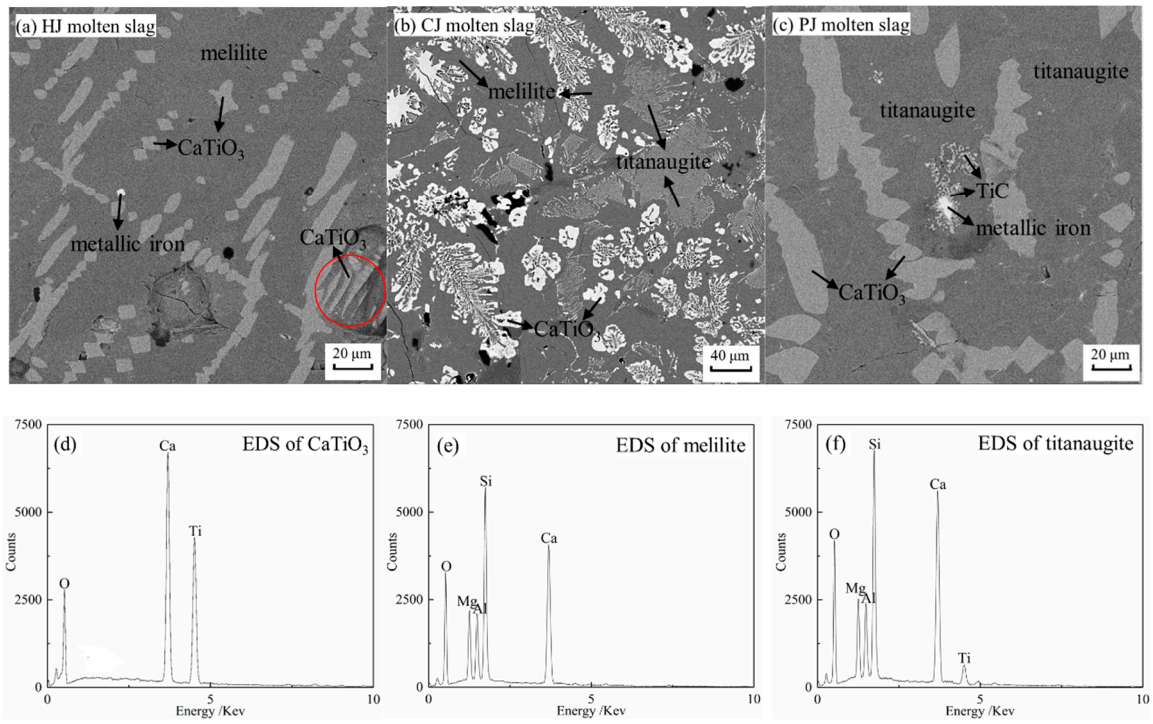

Figure 4. The SEM-EDS images of molten slag: (**a**) HJ molten slag; (**b**) CJ molten slag; (**c**) PJ molten slag; (**d**) EDS of $CaTiO_3$; (**e**) EDS of melilite; (**f**) EDS of titanaugite.

The SEM image of the non-dripping is shown in Figure 5. It can be seen that the blocky (Fe, V, Cr) and banded C are embedded in the metallic iron. The presence of C causes the metallic iron to become less fluid, so that it cannot drip from the crucible. Fe, V, and Cr aggregates are present in the non-dripping, resulting in a decrease in the recovery rate of valuable components.

The Richardson oxide free energy diagram of related elements is drawn using FactSage 7.0 software (ThermFact LTD, Montreal, QC, Canada), as shown in Figure 6. It can be seen that V_2O_3 and Cr_2O_3 cannot be directly (with C) reduced at temperatures below 1250 °C. Thus, they are present in wustite and $(Fe,Ti)O_x$. With the increase in temperature, the direct reduction of oxides is further carried out in the melting-dripping zone. The reaction equations are shown in Equations (4), (6) and (7). Vanadium and Chromium are contained in dripping and non-dripping. However, the reduction temperature of titanium oxide is so high that it cannot be reduced, and it reacts to form $CaTiO_3$ and titanaugite in the molten slag, as shown in Equations (8)–(9).

$$V_2O_3 + 3C = 2V + 3CO \quad (6)$$

$$Cr_2O_3 + 3C = 2Cr + 3CO \quad (7)$$

$$TiO_2 + CaO = CaTiO_3 \quad (8)$$

$$(Mg, Al)O_x \cdot TiO_2 + Silicate = Titanaugite \quad (9)$$

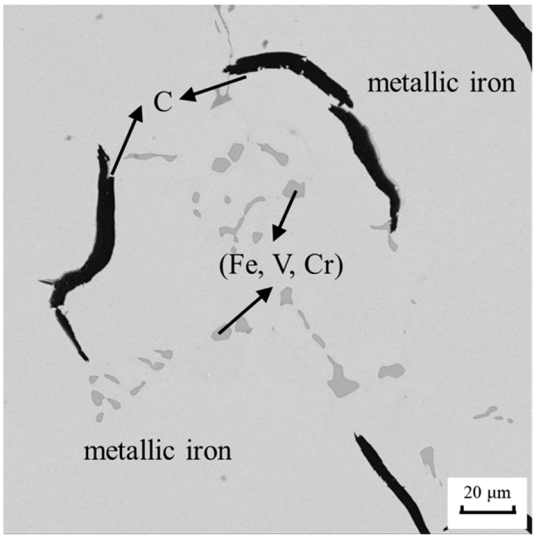

Figure 5. The SEM image of non-dripping.

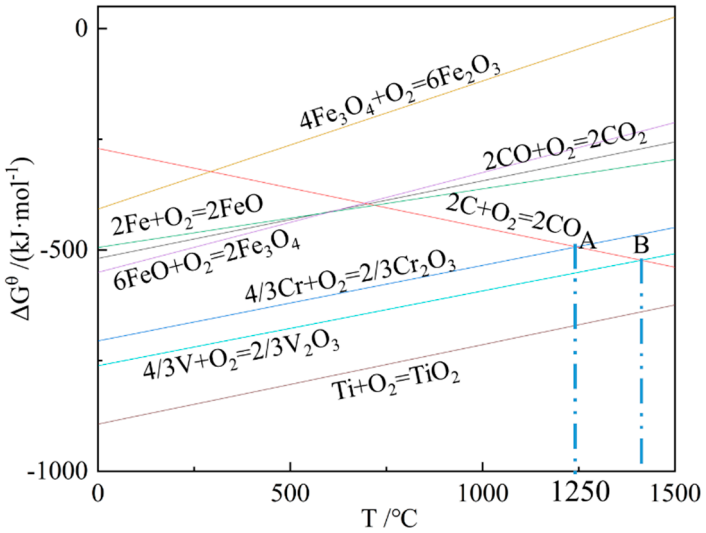

Figure 6. The Richardson oxide free energy diagram of related elements.

3.3. Softening-Melting-Dripping Performance

The softening-melting-dripping performance of the burden has a dramatic effect on the reduction process, and the permeability and distribution of gas there is also affected. In this work, softening start temperature (T_4), softening end temperature (T_{40}), melting start temperature (T_s), dripping temperature (T_d), and pressure drop (ΔP_m) are measured to evaluate the softening-melting-dripping properties. T_4 and T_{40} are the temperatures at which the shrinkage degree of the burden reaches 4% and 40%, respectively. T_s is the temperature when the gas pressure drop begins to increase rapidly. When the temperature reaches T_d, the molten iron drips from the crucible. The softening ($\Delta T_1 = T_{40} - T_4$) and melting ($\Delta T_2 = T_d - T_s$) zones need to be noted. Permeability index (S) is also an important characteristic value. S can be calculated by Equation (10).

$$S = \int_{T_s}^{T_d} (P_m - \Delta P_s) \quad (10)$$

where P_m is pressure difference at any time, Pa, and ΔP_s is the starting melting pressure difference, Pa.

The softening-melting-dripping characteristics of the burden are shown in Table 4. T_4

of the burden mainly depends on the melting point of the low melting point slag phase in the reduction process. T_4 and T_{40} are affected by so many factors, such as CaO, SiO_2, TiO_2, and burden structure, that no obvious pattern has been found. The high T_4 and narrow ΔT_1 are favorable for blast furnace smelting. It can be found that the PJ burden has the highest softening start temperature (T_4) and the narrowest softening zone (ΔT_1) of the three kinds of burden. Therefore, the softening property of the PJ burden is the best.

Table 4. Performance data of softening-melting-dripping of burden.

Content	T_4/°C	T_{40}/°C	$(T_{40} - T_4)$/°C	T_s/°C	T_d/°C	$(T_d - T_s)$/°C	ΔP_m/Pa	S/(kPa·°C)
HJ Burden	1082	1225	143	1272	1480	208	32766	2056.5
CJ Burden	1121	1255	134	1269	1471	202	22288	2042.1
PJ Burden	1130	1211	81	1226	1490	264	22685	2532.9

In Table 4, it can be found that Ts is closely related to the content of TiO_2 in the burden as seen in Figure 7. With the increase of TiO_2 content, Ts decreases gradually. When the content of TiO_2 in the burden begins to increase, although more high-melting-point $CaTiO_3$ and titangarnet will be generated, the low-melting-point titanaugite also increases. Titanaugite increases permeability resistance at lower temperatures, leading to a decrease in Ts to a certain extent. PJ burden has the highest T_d and the widest ΔT_2. This is because TiO_2 increases the viscosity of slag and affects the drop of molten iron. When the appropriate fluidity is reached by increasing the temperature, the molten iron drips smoothly. A lower Ts and a wider ΔT_2 are disadvantageous in blast furnace smelting.

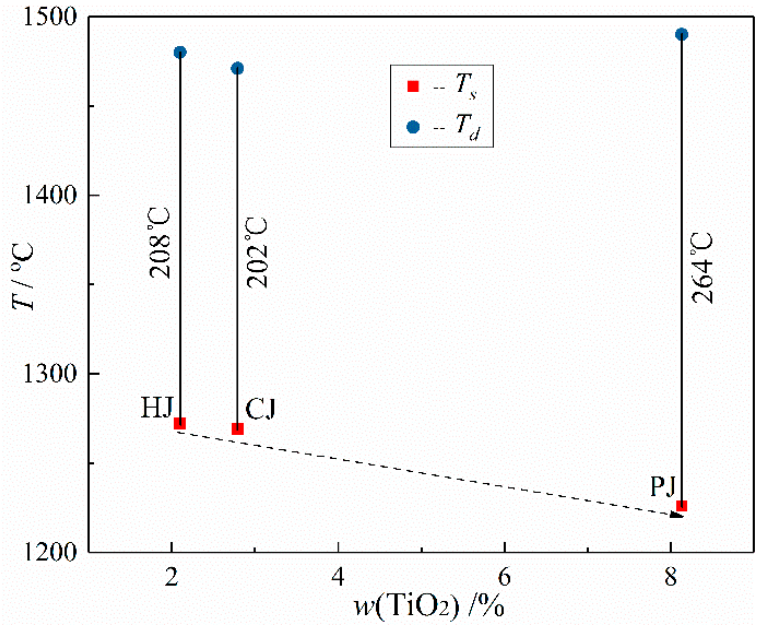

Figure 7. Relationship between Ts, Td, and TiO_2 content of burden.

The results of the permeability index (S) are shown in Table 4. The smaller the S, the better the droplet performance. It can be seen that the S of the PJ burden is much larger than the others, and that its permeability is the worst.

Figure 8 shows the dripping mass of the HJ, CJ, and PJ burden. It can be found that the dripping mass is inversely proportional to the content of TiO_2 in the burden. When the content of TiO_2 is high, the metallic iron is wrapped by the surrounding Ti(C,N), resulting in the loss of dripping. In addition, reducibility is also an important factor affecting the drop of molten iron. The poor reduction of the burden increases the reduction process and difficulty. The pellet ratio of PJ burden with good reducibility is the lowest, so its dripping mass is the lowest.

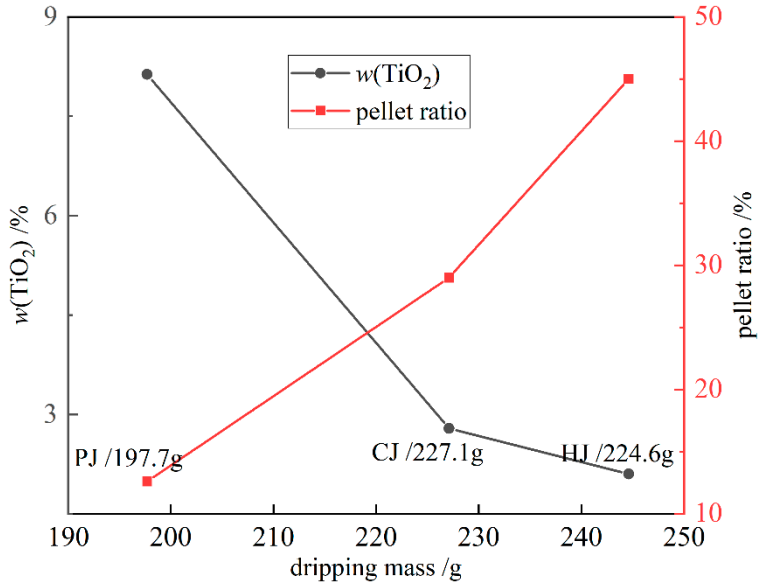

Figure 8. Relationship between dripping mass, TiO_2 content, and pellet ratio of burden.

4. Conclusions

In this study, the soft slag, molten slag, non-dripping and dripping were analyzed by SEM-EDS. The reduction behavior and softening-melting-dripping performance of the burden was investigated in a cohesive and a melting-dripping zone. The conclusions are as follows:

(1) Iron oxides are reduced in the cohesive zone. Wustite and coated $(Fe,Ti)O_x$ are formed in the core of pellet and sinter, while iron oxides and $CaFeSiO_4$ at the periphery is reduced to formed metallic iron and $CaSiO_3$.

(2) With the different content of TiO_2 in the burden, the substrate phase of the molten slag is different. The aggregate (Fe, V, Cr) exists in the non-dripping, and metallic iron wrapped by TiC exists in the molten slag, which causes the loss of valuable components.

(3) The mass of the dripping is directly proportional to the pellet ratio and is inversely proportional to the TiO_2 content.

(4) PJ burden with high TiO_2 content has a high T_d and a wide ΔT_2, which is not conducive to blast furnace smelting.

Author Contributions: Conceptualization, X.X., K.C. and Z.H.; methodology, Z.H., J.L. and G.C.; validation, X.X., X.H. and Z.H.; formal analysis, Z.H. and M.L.; investigation, Z.H.; data curation, Z.H.; writing—original draft preparation, Z.H.; writing—review and editing, Z.H.; supervision, X.X.; project administration, X.X. and X.H.; funding acquisition, X.X. and X.H. All authors have read and agreed to the published version of the manuscript.

Funding: This research was funded by the National Natural Science Foundation of China (Grant No. U1908226, No. 51674084, and No. 21908020).

Data Availability Statement: Data is contained within the article.

Conflicts of Interest: The authors declare no conflict of interest.

References

1. Yang, S.T.; Zhou, M.; Tang, W.D.; Jiang, T.; Xue, X.X.; Zhang, W.J. Influence of coke ratio on the sintering behavior of high-chromium vanadium–titanium magnetite. *Minerals* **2017**, *7*, 107. [CrossRef]
2. Cheng, G.J.; Gao, Z.X.; Yang, H.; Xue, X.X. Effect of calcium oxide on the crushing strength, reduction, and smelting performance of high-chromium vanadium-titanium magnetite pellets. *Metals* **2017**, *7*, 181. [CrossRef]
3. He, Z.W.; Yue, H.R.; Xue, X.X. Study of the high temperature metallurgical properties of on-site samples with vanadium-titanium magnetite. *Trans. Indian Inst. Met.* **2018**, *71*, 2001–2013. [CrossRef]

4. Kemppainen, A.; Ohno, K.; Iljana, M.; Mattila, O.; Paananen, T.; Heikkinen, E.; Maeda, T.; Kunitomo, K.; Fabritius, T. Softening behaviors of acid and olivine fluxed iron ore pellets in the cohesive zone of a blast furnace. *ISIJ Int.* **2015**, *55*, 2039–2046. [CrossRef]
5. Tang, W.D.; Yang, S.T.; Cheng, G.J.; Gao, Z.X.; Yang, H.; Xue, X.X. Effect of TiO_2 on the sintering behavior of chromium-bearing vanadium-titanium magnetite. *Minerals* **2018**, *8*, 263. [CrossRef]
6. Park, E.; Ostrovski, O. Effects of preoxidation of titania-ferrous ore on the ore structure and reduction behavior. *ISIJ Int.* **2004**, *44*, 74–81. [CrossRef]
7. Yang, S.T.; Tang, W.D.; Zhou, M.; Jiang, T.; Xue, X.X.; Zhang, W.J. Effects of dolomite on mineral compositions and metallurgical properties of chromium-bearing vanadium–titanium magnetite sinter. *Minerals* **2017**, *7*, 210. [CrossRef]
8. Zhou, L.H.; Zeng, F.H. Reduction mechanisms of vanadium-titanomagnetite-non-coking coal mixed pellet. *Ironmak. Steelmak.* **2011**, *38*, 59–64. [CrossRef]
9. Zhen, Y.L.; Zhang, G.H.; Chou, K.C.; Mills, K. Influence of TiN on viscosity of CaO-MgO-Al_2O_3-SiO_2-(TiN) suspension system. *Metall. Trans. B* **2015**, *54*, 340–348. [CrossRef]
10. Zhang, L.H.; Yang, S.T.; Tang, W.D.; Xue, X.X. Investigations of MgO on sintering performance and metallurgical property of high-chromium vanadium-titanium magnetite. *Minerals* **2019**, *9*, 324. [CrossRef]
11. Frohlichova, M.; Findorak, R.; Legemza, J. Structural analysis of sinter with titanium addition. *Arch. Metall. Mater.* **2013**, *58*, 179–185. [CrossRef]
12. Fu, W.G.; Xie, H.E. Progress in technologies of vanadium-bearing titanomagnetite smelting in PanGang. *Steel Res. Int.* **2011**, *82*, 501–504. [CrossRef]
13. Cheng, G.J.; Xue, X.X.; Jiang, T.; Duan, P.N. Effect of TiO_2 on the Crushing Strength and Smelting Mechanism of High-Chromium Vanadium-Titanium Magnetite Pellets. *Metall. Trans. B* **2016**, *47*, 1713–1726. [CrossRef]
14. Zhou, M.; Jiang, T.; Yang, S.T.; Xue, X.X. Sintering behaviors and consolidation mechanism of high-chromium vanadium and titanium magnetite fines. *Int. J. Min. Met. Mater.* **2015**, *22*, 917–925. [CrossRef]
15. Yue, H.R.; He, Z.W.; Jiang, T.; Duan, P.N.; Xue, X.X. Rheological evolution of Ti-bearing slag with different volume fractions of TiN. *Metall. Trans. B* **2018**, *49*, 2118–2127. [CrossRef]
16. Yue, H.R.; Jiang, T.; Zhang, Q.Y.; Duan, P.N.; Xue, X.X. Electrorheological effect of Ti-bearing blast furnace slag with different TiC contents at 1500A degrees C. *Int. J. Min. Met. Mater.* **2017**, *24*, 768–775. [CrossRef]
17. Wei, W.; Yue, H.R.; Xue, X.X. Diffusion coefficient of Ti(4^+)in calcium ferrite/calcium titanate diffusion couple. *Int. J. Min. Met. Mater.* **2020**, *27*, 1216–1225. [CrossRef]
18. Ledzki, A.; Migas, P.; Stachura, R.; Klimczyk, A.; Bernasowski, M. Chemical and phase characteristics of titanium compounds produced in iron blast furnace dripping zone. *Arch. Metall. Mater.* **2009**, *54*, 129–135.